

GT-2003-38025

INTERACTION OF SHROUD LEAKAGE FLOW AND MAIN FLOW
 IN A THREE-STAGE LP TURBINE

Jochen Gier Bertram Stubert
 Bernard Brouillet Laurent de Vito

MTU Aero Engines
 Munich, Germany

ABSTRACT

Endwall losses significantly contribute to the overall losses in modern turbomachinery, especially when aerodynamic airfoil load and pressure ratios are increased. In turbines with shrouded airfoils a large portion of these losses are generated by the leakage flow across the shroud clearance. Generally the related losses can be grouped into losses of the leakage flow itself and losses caused by the interaction with the main flow in subsequent airfoil rows.

In order to reduce the impact of the leakage flow and shroud design related losses a thorough understanding of the leakage losses and especially of the losses connected to enhancing secondary flows and other main flow interactions has to be understood. Therefore, a three stage LP turbine typical for jet engines is being investigated.

For the three-stage test turbine 3D Navier-Stokes computations are performed simulating the turbine including the entire shroud cavity geometry in comparison with computations in the ideal flow path. Numerical results compare favourably against measurements carried out at the high altitude test facility at Stuttgart University. The differences of the simulations with and without shroud cavities are analysed for several points of operation and a very detailed quantitative loss breakdown is presented.

NOMENCLATURE

A	[m ²]	area
C _{e2} , C _μ	[-]	constants
C _c	[-]	Contraction coefficient
g	[m]	clearance gap
h	[m]	airfoil height

\dot{m}	[kg/s]	mass flow rate
p	[Pa]	pressure
r	[m]	radius
s	[kJ/(kg K)]	entropy
T	[K]	temperature
y	[m]	wall distance
v	[m/s]	velocity
α	[°]	flow angle (from axis)
μ	[Pa s]	dynamic viscosity
η	[-]	efficiency
ρ	[kg/m ³]	density
ω	[1/s]	specific turbulence dissipation
ζ	[-]	enthalpy loss coefficient
ζ_s	[-]	entropy loss coefficient $= (T_2 \Delta s)/(h_{t2} - h_2)$

Subscripts

C	Carnot
L	leakage
m	main flow
is	isentropic
t	total
w	wall
x	axial
Θ	circumferential
1	inlet
2	exit

INTRODUCTION

Shrouded airfoils are widely used in many turbines of different applications. In aero engines the low pressure turbine is generally

build with shrouded airfoils. Although clearances of modern turbines are generally quite small, leakage flow related losses still contribute significantly to the overall losses of a turbine.

Much research has been undertaken in the past focussing on the flow inside the labyrinth seals aimed at understanding and optimising the labyrinth discharge coefficients (Egli, [1], Rhode et al. [2a,b], Takenaga et al. [3]). Millward and Edwards [4] investigated windage heating in labyrinth seals.

Denton and Johnson [5] presented two-dimensional experimental data for the flow over a shrouded steam turbine. Recently a number of investigations addressed the connection between the cavity leakage flow and the main flow in turbines. Pfau et al. [6] performed detailed experimental investigations on the flow structure at the exit of an annular cascade. They found changes in the main flow exit angle compared to a configuration without leakage flow and pitchwise variation in the re-entering flow.

Peters et al. [7] performed experimental investigations in a 1-1/2 stage low-speed axial turbine with a tip cavity above the rotor. They also reported indications of circumferentially non-uniform cavity exit flow and a significant negative incidence to the following stator. Similar effects on the subsequent stator were described by Anker and Mayer [8] for the same configuration. Kortschunov and Döhler [9] investigated the effect of artificial jets in a linear cascade.

Hunter and Manwaring [10a,b] performed an extensive experimental and numerical investigation on the flow in the cavity – main flow connection for a hub cavity in a 2-stage low-speed test rig. They found significant changes in the flow fields of the two rows downstream of the first vane and its inner air seal. The low momentum of the cavity flow re-entering into the main flow path and mixing with the main flow was entrained into the first rotor secondary flow and transported radially up to 7.5% span of this high aspect ratio airfoil.

A more general discussion of cavity related effects including losses can be found in Traupel [11] and Denton [12]. The descriptions of the losses given in these publications concentrate on losses caused by the leakage and the mixing of the cavity flow with the main flow. Denton provides a number of relations for the leakage flow fraction as well as the related mixing losses based on the assumption of constant circumferential velocity in the cavity flow.

Wallis et al. [13] performed investigations on a tip cavity configuration in a 4-stage axial turbine. They report four different losses connected with the cavity flow: The cavity entry, the clearance gaps, the mixing with the main flow and the incidence on the following row. They aimed at reducing losses by reducing the mixing losses with the main flow. Therefore, different turning devices were designed and tested, which reduced the flow angle difference of the cavity flow and the main flow. However, all of the turning devices resulted in an efficiency drop compared to the reference configuration.

There is also quite a number of papers focussing on the effects of coolant flows on the main flow especially for high pressure turbines, e.g. McLean et al. [14a,b], Girgis et al. [15]. A common result of these investigations is the significance of interaction effects of the injection flow with the main flow and the related losses, which can amount up to 1 % or 2 % in efficiency. There are also a number of compressor

cavity studies indicating a comparable significance and complexity of shroud leakage flows, e.g. [16, 17, 18].

Most of the previous studies discussed above focuses either on some of the interaction phenomena between leakage flow of shrouded turbines or on estimates of losses. This paper builds upon this background to construct a more complete picture of the interaction between leakage and main flow and the resulting losses in shrouded turbines. This is done for a test turbine, which is typical for low pressure turbines in aero engines. For this investigation numerical simulation is employed and compared to experimental measurements carried out in the main flow.

Since in a real aero engine this turbine would follow a 2-stage high pressure turbine the airfoil numbering starts with Vane 3 (V3).

NUMERICAL METHOD

The simulations are performed with the TRACE_S 3D compressible Navier-Stokes code, which is based on a block-structured finite volume scheme. The code computes the multiple rows fully coupled. Time integration for this investigation is done using an implicit procedure to reach steady state conditions. The convective fluxes are computed with a higher order MUSCL scheme combined with the flux differencing method of Roe. Convective fluxes are limited with a special version of the Van Albada Limiter. For the diffusive fluxes a central scheme is employed.

The stage coupling is based on the mixing plane technique with flux averaging and non-reflecting boundary interfaces and full mass conservation. The code is vectorised and parallelised. More the numerical details can be found in Fritsch et al. [19].

Turbulence Modeling

The investigated turbine operates at Reynolds numbers typical for jet engine conditions. Thus a reliable representation of turbulence in the boundary layers is important. Therefore, the Wilcox $k-\omega$ [20] two-equation model in low-Reynolds version was employed with extensions for compressibility and system rotation. Since the model does not need wall distances it appears relatively well suited also for complex cavity geometries.

The equations are time-discretized by 2 x 2 block-implicit time stepping. The resulting system of equations is solved with a Gauss-Seidel algorithm. For more details please refer to Gier et al. [21].

Transition Modeling

Since the flow in a low pressure turbine is significantly governed by laminar-to-turbulent transition, a transition model is employed in combination with the $k-\omega$ turbulence model for this investigation. It is based on the correlations of Abu-Ghannam and Shaw [22] with modifications of Drela [23]. It was selected from the variety of different models, because it takes the boundary layer shape and thus the pressure gradients into account. It is also dependent on the free-stream turbulence level, which is taken from the local turbulence level at the boundary layer edge provided by the turbulence model. Further details with additional references are given in [21] and [24].

Mesh Generation

The mesh covering both the main flow channel and the cavities is made of structured grids exclusively. This allows the use of the same

CFD solver as for the current design applications at MTU. The grid is generated in a rather automatic way in three steps:

1. Cavities

Thanks to the axisymmetry of the present cavities, the grids are first defined in the 2D plane (x,r) and then they are extended in the pitchwise direction to form a 3D volume. The 2D definition is done in a semi-automatic mode directly in the CAD environment. The (x,r) contours of the intersections with the main flow channel and of the main flow mixing planes are exported from the CAD tool and transmitted to the grid generator for the main flow channel (red and green lines in figure 2). A view of the complete geometry can be seen in figure 1.

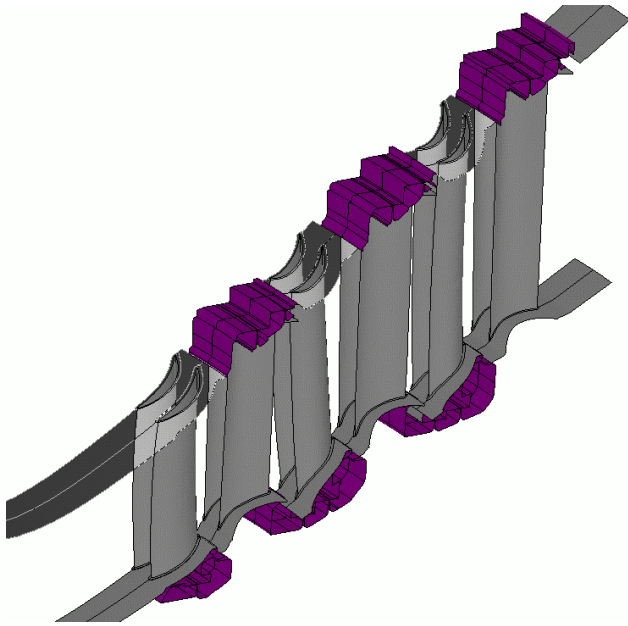


Figure 1: View of test turbine with modelled cavities

2. Main flow channel

The computational mesh for the main flow channel consists of 12 blocks. Each vane or blade is gridded with one O-type grid around the airfoil and a H-type grid for the major part of the channel. At hub and tip, the grid is limited by contour from the CAD tool.

3. Merging process and definition of intersections

While merging the different grid blocks, the connectivity of the different parts is inherited and put together automatically. Thus, only the interfaces between the associated parts have to be defined. When joining grids (main flow and cavity) rotate alike and have the same pitch, an abutting interface is defined and the solver is told to interpolate the aerodynamic data on both sides. When joining grids do not rotate alike but exhibit an axisymmetric structure at the common surface, the identical mixing plane technique as between two adjacent rows is used to exchange aerodynamic data.

4. Grid resolution

For resolving small flow features and to assure a dimensionless wall distance y^+ towards the blade profiles of about 1 the boundary layer grid is heavily clustered close to the surface. The resulting number of grid nodes in a row passage is approximately 600,000 with 65 nodes in radial and 69 nodes in circumferential direction. The total

number of grid nodes for the main flow channel is about 3.6 million, for the configuration with cavities 4.2 million (220 blocks).

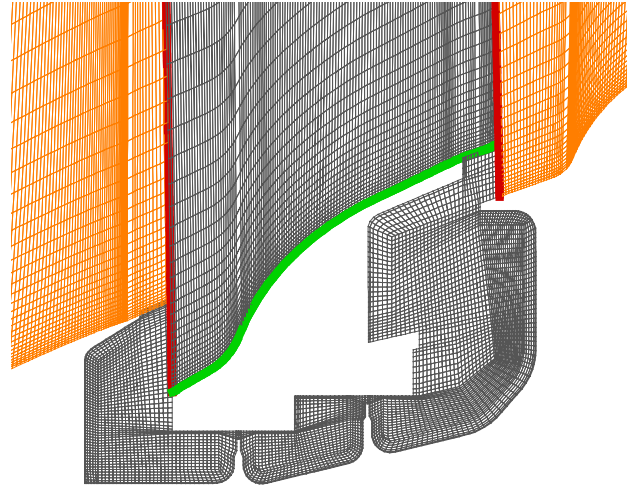


Figure 2: Mesh in third vane inner air seal (IAS2)

Boundary Conditions

Non-reflecting boundary conditions are applied at inlet and outlet. Measured total pressure, total temperature and flow angle distributions are prescribed at the inlet and static pressure at the outlet. The inlet turbulence intensity is below 1 % which is lower than in a real engine because of the specific test rig configuration.

At solid walls velocities are set to zero except for rotating walls. All walls are assumed to be adiabatic. Turbulent kinetic energy is set to zero and the specific dissipation rate ω is determined according to:

$$\omega_w = \frac{6\mu_w}{(C_{e2} - 1) \cdot C_\mu \rho y_w^2} \quad (1)$$

At the endwalls a fully turbulent flow regime is to be expected. Therefore, a wall function formulation according to Spalding is employed here as well as within the cavities, enabling the use of a somewhat coarser endwall grid resolution without a significant loss in accuracy and thus reducing the computational effort noticeably.

All results were accepted as converged, when massflow and efficiency of the component and the individual stages remained constant within very sharp limits and with residuals down by at least 2 orders of magnitude. For the cavity computations this leads to significant convergence time increases due to the slow convergence of the energy equation in the slowly moving and strongly recirculating flows inside the cavities.

IMPACT OF CAVITY MODELLING

Comparison with Experimental Data

To assess the quality of the numerical simulation as well as to judge the differences between computations geometrically modelling the cavities and computations in the ideal flow path, some comparison examples are discussed in this section. In figure 3 the static pressures

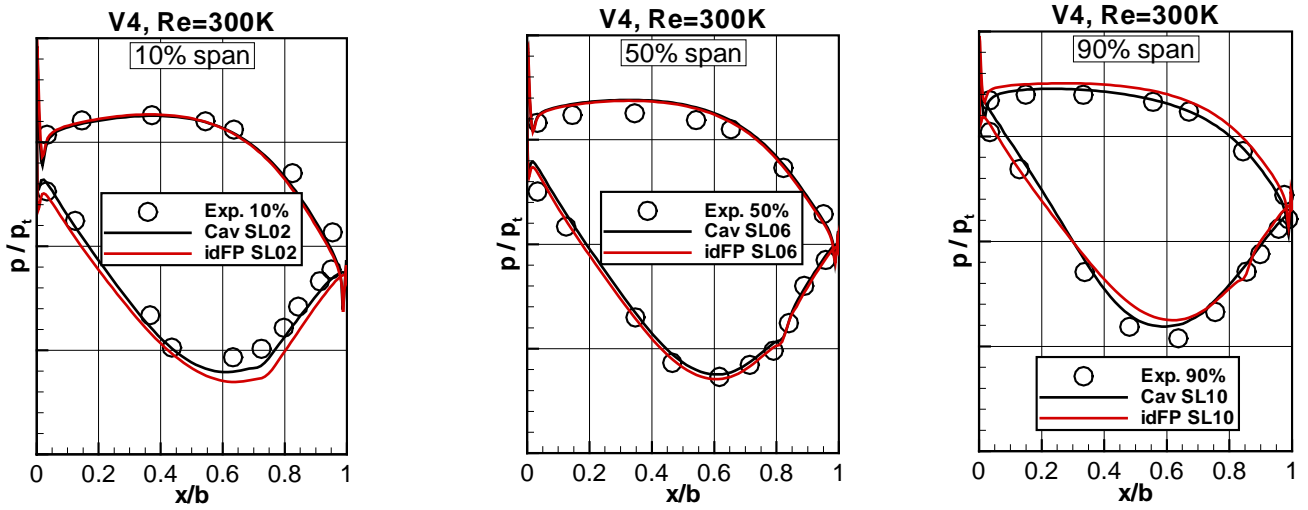


Figure 3: Static pressure in second vane (V4) for cavity and ideal flow path computations

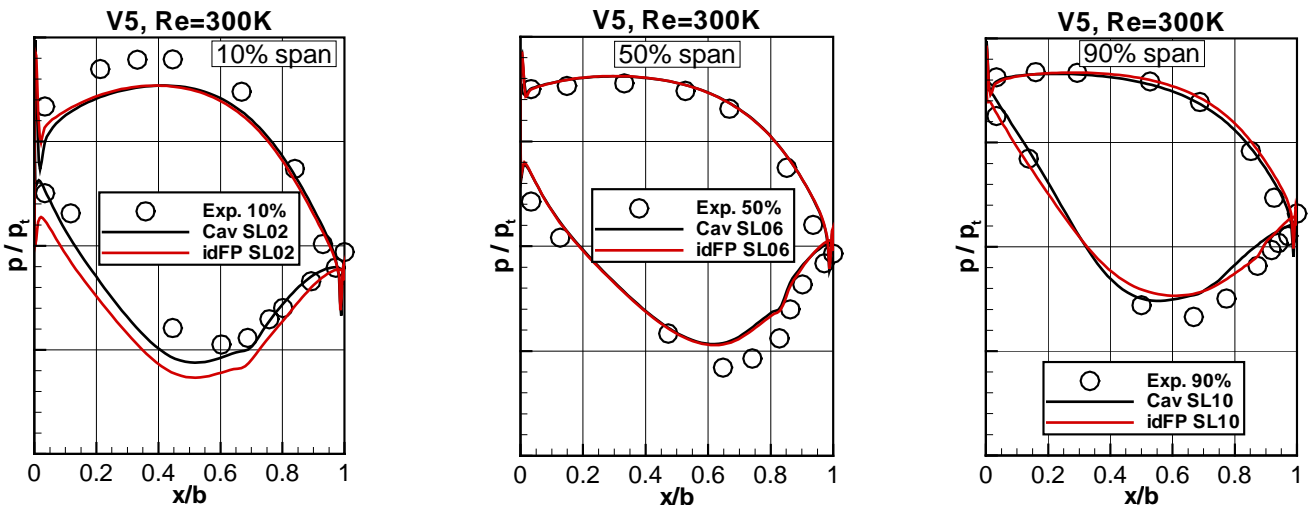


Figure 4: Static pressure in third vane (V5) for cavity and ideal flow path computations

on the middle guide vane (V4) are plotted at the 3 radial locations that were instrumented.

At midspan the difference between the two computations is marginal with a slightly smaller load for the cavity computation. This is caused by the by-pass of mass through the inner air seal of this vane. Both distributions correspond quite well to the experimental data. In the tip region the cavity computation exhibits a stronger negative incidence, which results in a larger peak Mach number, which is in accordance with the data. Also the separation bubble, appearing in the ideal flow path computation at 80 % axial chord is suppressed in the cavity computation. At the hub section at 10% span the aerodynamic load of the cavity computation is smaller than for the ideal flow path. This gives a better agreement with the experiment. The reason is the by-pass of flow through the inner air seal.

In the third vane, shown in figure 4, the same trends can be observed at the three radial locations. In total the pressure distributions in this vane seem to be a little bit unloaded, which besides computation accuracy might be also due to hardware deviations. Still the simulation and experiment correspond reasonably well for this vane.

In figure 5 radial distributions of the isentropic efficiency are plotted for the three Re-numbers investigated. For the intermediate Re-number of 300,000 a computation of a configuration with half the clearances is added. For all Re-numbers it becomes evident that the efficiency in the core flow is hardly affected by the presence of the cavity leakage flow. However, it is strongly affected up to 25 % span from the endwalls. General agreement is considerably better for the cavity computations, although especially at the hub the efficiency drop is somewhat overpredicted. Also the computed efficiency is too high between 60 % and 70 % span. The reason for this is not yet understood. Possibly radial mixing is stronger than computed or turbulence is not adequately modelled in this region. The main flow radial gradient of the total pressure is also reasonably well captured by all computations (Fig. 5). The cavity computations exhibit a little bit thicker boundary layer.

The difference between the ideal flow path and the cavity computations is limited in terms of airfoil flow structure in the core flow as can be seen in figure 6. Here the computed flow streamtraces in the vicinity of the airfoil are compared to flow visualization in the test rig for different airfoils of the vane 4 row (Pos.1 & Pos. 2). In the

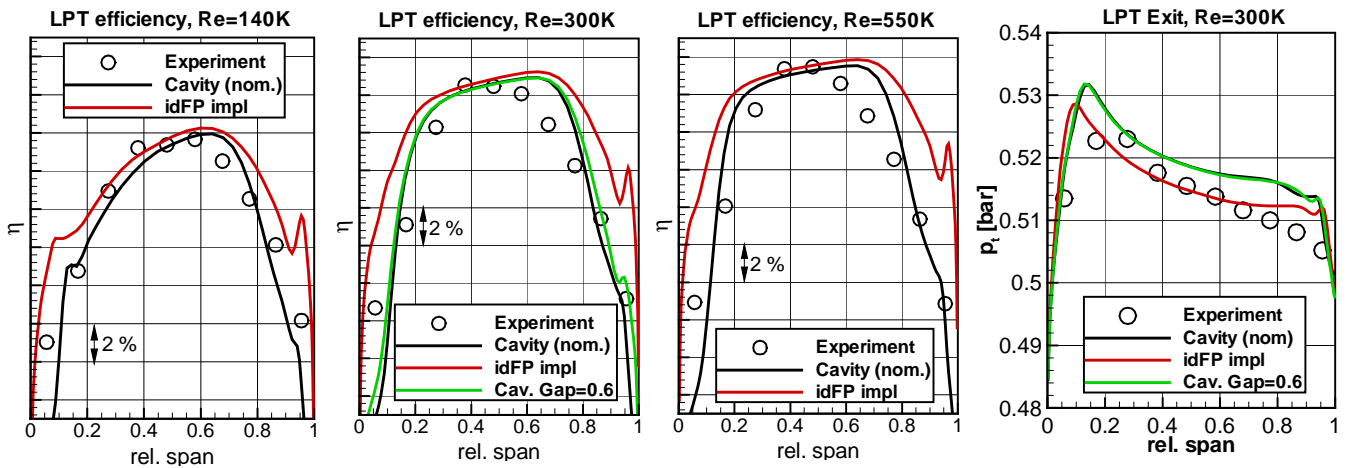


Figure 5: Isentropic efficiency distribution and exit total pressure for cavity and ideal flow path in comparison to experimental data

computation the separation bubble is quite well captured in terms of the streamwise extent as well as the radial extent. Taking a detailed look it appears that the ideal flow path computation tends to form a small bubble at about 80 % span (location A) while the cavity computation does not. The reason seems to be that in the cavity computation the secondary flow is stronger and is radially extending further into the main flow. This is indicated by the stronger radial slope of the streamtraces in area B in figure 6.

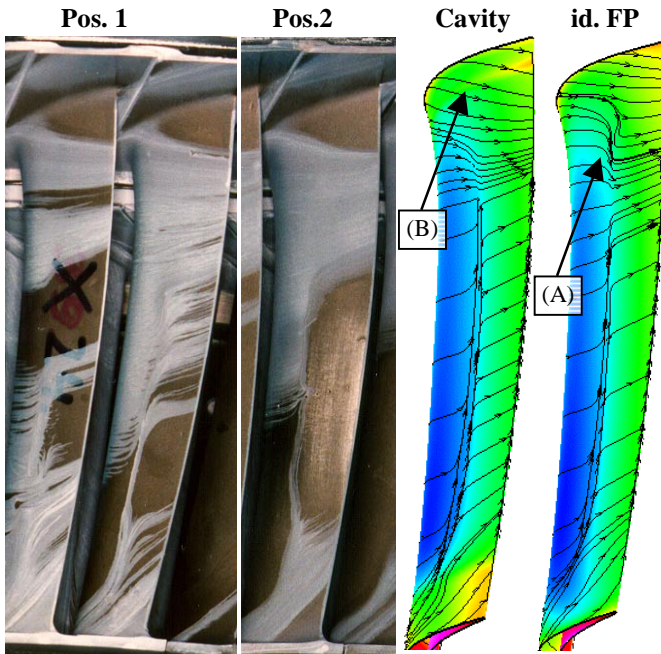


Figure 6: Streamtraces on vane 4 (V4)

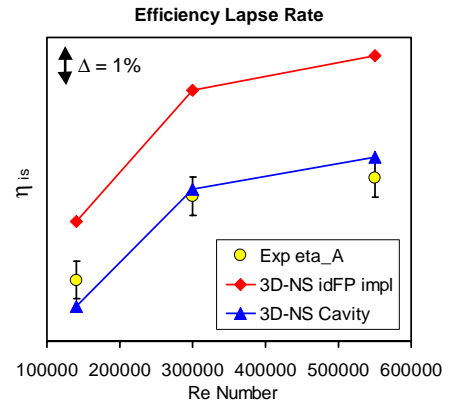


Figure 7: Turbine efficiency Reynolds number lapse rate

The reduction of the efficiency in the endwall regions between ideal flow path and cavity computation for this turbine is fairly large (Fig. 7). At design Reynolds number (300K) this difference is about 2.6 %, somewhat reducing to about 2.2 % at the low Reynolds number. This effect is discussed further below. The overall efficiency level of the cavity computation is close to the experimental data, however the efficiency lapse is overpredicted. This effect is likely to be ascribed to the transition modelling, which produces too large suction side separation bubbles at the lowest Reynolds numbers.

Plausibility and general features of leakage flow

Inside the inner and outer air seals a complex flow structure, driven by the leakage flow, develops. The flow structure developing inside the hub cavity is displayed in figure 8 for both clearances. In this figure a meridional slice is displayed. Since circumferential variations are relatively small inside the cavities, this distribution is representative for the entire circumference. The flow enters the cavity upstream of the second vane through a large vortex. There are several vortices formed inside the cavity by the complex geometry and clearance fins. Finally the leakage flow re-enters the main flow through the gap between second vane and blade. Here an additional vortex is formed, which like the entrance vortex turns clockwise. These two vortices fill the gap between the adjacent airfoil rows.

Reducing the clearance by half from 1.2 mm to 0.6 mm reduces the leakage flow through the cavity also approximately by half. By inspection of figure 8 it can be seen that this does not change the flow structure. However, the entrance vortex and the exit vortex grow a little bit. At the exit the vortex grows especially axially forwards, which squeezes the exiting leakage flow and reduces its axial flow component. Also the entropy level in the rear part of the cavity rises. This makes sense, because in the case of the smaller gap less lower entropy fluid coming from the main flow flushes the cavity while the windage losses generation inside the cavity basically remains constant.

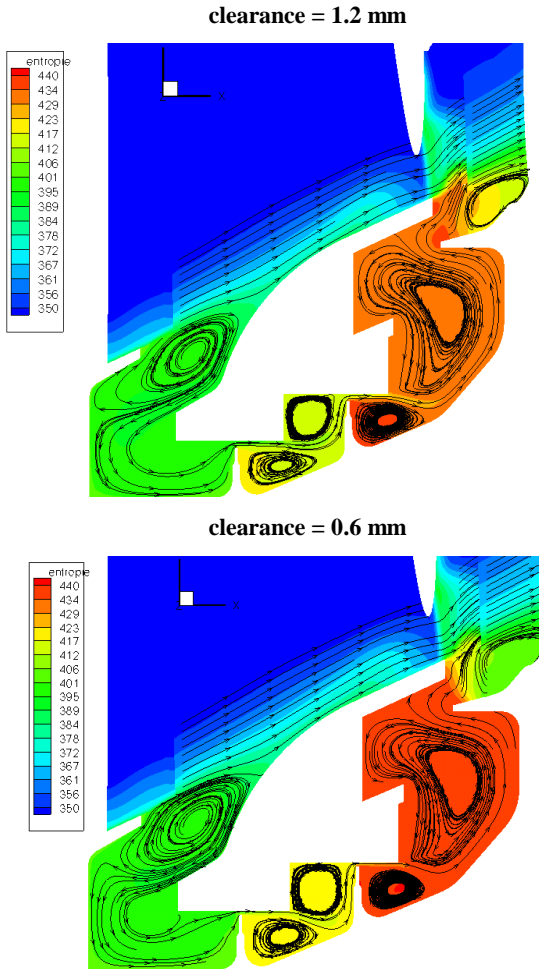


Figure 8: Flow structure and entropy in inner air seal IAS2 for 2 clearances, Re = 300,000 (projection into meridional plane)

At the outer air seal a similarly complex flow structure develops (fig. 9). The leakage flow is entering the outer air seal through the downstream side of the large entrance vortex upstream of the second rotor leading edge. The flow is then turned and driven through the clearance seals, forming additional vortices. It eventually leaves the cavity relatively smoothly by forming two smaller exit vortices. The smaller clearance case is very similar, hardly exhibiting any change in the extent of the vortices.

In figure 10 the hub contour of the second vane is shown. On the left side a photograph with colour traces from experiment and on the right side the equivalent simulation result are displayed. Besides the

nice agreement of the passage vortex driven hub streamlines in the rear part of the passage special focus should be put onto the front part. Here the same stagnation line in circumferential direction is present in experiment as well as in the computation. Both the position and the structure with a stagnation point about two thirds of the pitch towards the airfoil pressure side are well captured. The presence of the airfoil passage causes some circumferential inhomogeneity of the recirculating flow in the entrance vortex upstream of the stagnation line.

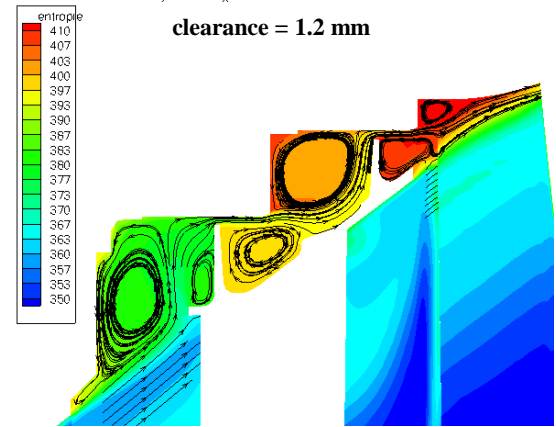


Figure 9: Flow structure and entropy in outer air seal OAS2 for 1.2 mm clearances, Re = 300,000 (projection into meridional plane)

Another important plausibility check is the evaluation of the leakage flow rates. These are shown in figure 11. Except for the first inner air seal (IAS1) below the first vane, which was closed in experiment and simulation, all seals have leakage flow fractions between 0.4 % and 0.75 % of total flow. The clearances are basically identically 1.2 mm and thus the relative gaps (clearance / airfoil span) through the turbine are slightly decreasing. However, the leakage flow through the inner air seals is significantly smaller. The obvious reason is the smaller relative area of the inner air seal gaps compared to the outer air seals. In addition the higher pressure ratio of the second inner air seal (vane 4 = row 3) compared to the third IAS (vane 5 = row 5) is seen to be responsible for the somewhat larger leakage flow in the second IAS despite its smaller relative gap area.

Denton [12] reports an estimate of leakage losses in shrouded turbines based on simple analysis. Assuming constant axial velocity, which is also a fairly good approximation for this test turbine, the relative leakage flow is:

$$\frac{\dot{m}_L}{\dot{m}_m} = \frac{g}{h} C_c \sqrt{\sec^2 \alpha_2 - \tan^2 \alpha_1} \quad (2)$$

	1 gap	2 gaps	CFD (Re=300K)
	m_L/m_m [%]	m_L/m_m [%]	m_L/m_m [%]
B3	1.37	0.97	0.69
B4	1.01	0.71	0.73
B5	0.94	0.66	0.73
V4	0.69	0.49	0.47
V5	0.81	0.57	0.38

Table 1: Relative leakage flow based on equation (2)

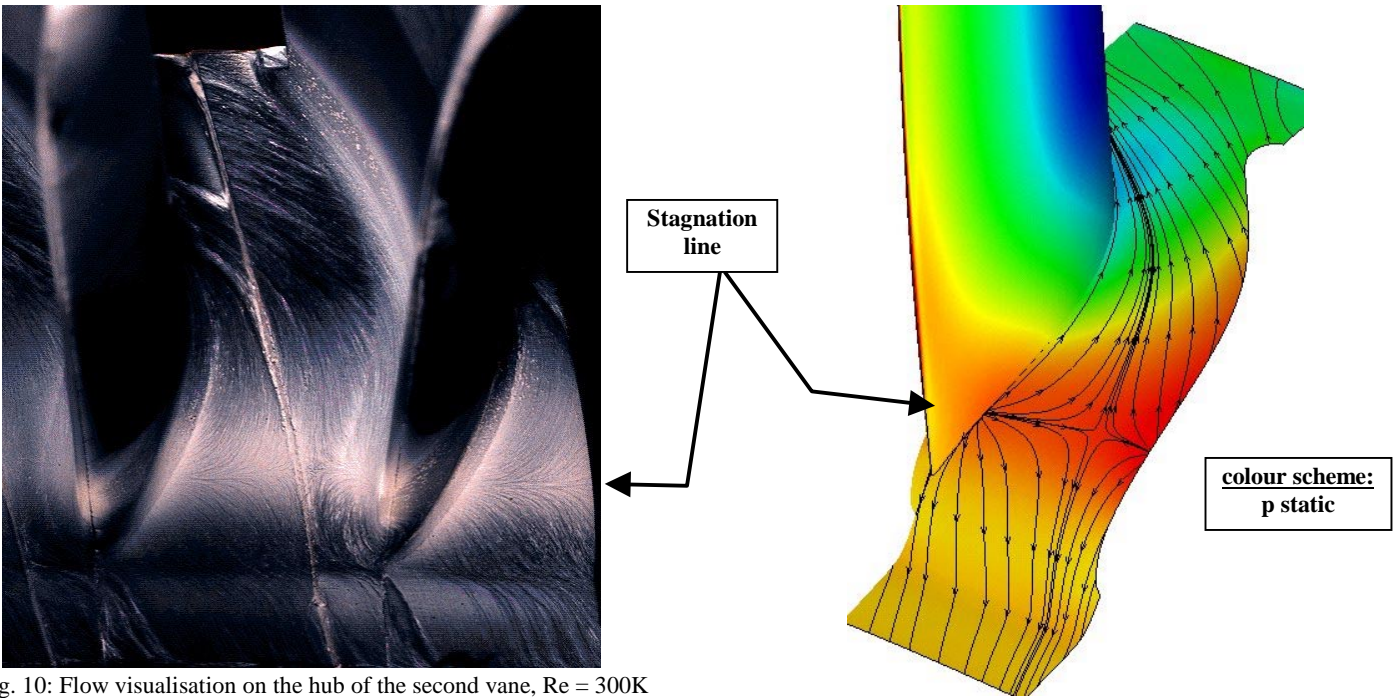


Fig. 10: Flow visualisation on the hub of the second vane, Re = 300K

Using a typical contraction coefficient C_c of 0.6 this formula gives the relative leakages shown in table 1. Comparing these with the cavity computation (Fig. 11, Table 1 right column) shows a reasonable agreement, when the value coming out of equation (2) is divided by $\sqrt{2}$ for taking 2 clearances per cavity into account (2 gaps). Except for the first blade (B3), where the value out of equation (2) is somewhat higher the leakage levels are quite similar and the difference between hub and casing seals is captured. However, this is only the case when the relative gap areas are taken for g/h and not the relative gaps themselves. Also the trends are not captured well.

up. At the lower Reynolds numbers the losses occurring in the main flow increase by increased friction and enlarged suction side boundary layer growth including separation bubbles. The flow structure in the cavities however is hardly affected by the Reynolds number and thus the flow blockage also hardly changes. The increased blockage in the main flow and the basically constant blockage in the leakage flow must result in an increase of leakage flow fraction with decreasing Reynolds number. This turns out to be the case as can be seen in figure 12.

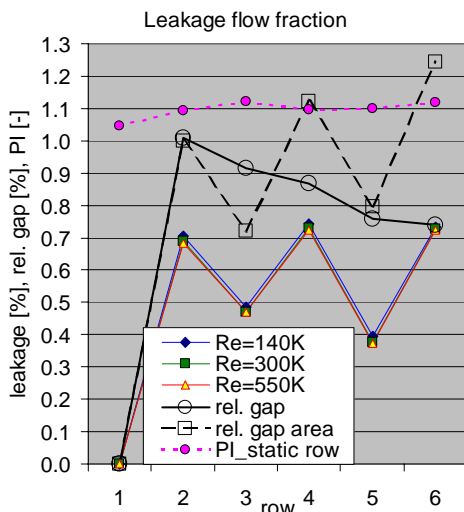


Figure 11: Leakage flow fraction, relative gap, relative gap area and static pressure ratio for all airfoil seals.

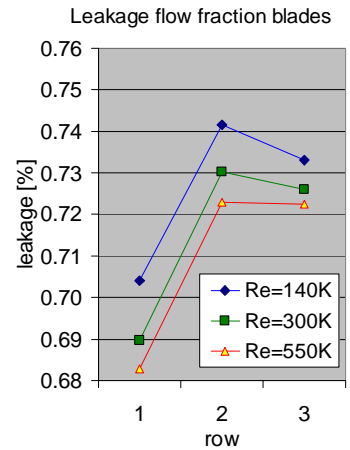


Figure 12: Leakage flow in OAS for different Reynolds numbers

To conclude this chapter, the authors feel that the current numerical simulation not only exhibits a good agreement with the experimental data but also the computed flow features in the not instrumented cavity regions correspond to engineering experience.

Finally one interesting detail should be addressed. In figure 12 the relative leakage flows through the outer air seals are shown in a close-

EFFECTS OF INTERACTION BETWEEN CAVITY- AND MAIN-FLOW

Cavity flows and the main flow interact in the region where the flow enters and leaves the cavity (Fig. 8, 9 and 10). Also the pressure distributions of the vanes in figures 3 and 4 show an increased negative incidence. This negative incidence can also be seen in figure 13. Close to the endwalls this amounts up to 5 degrees. Depending on the airfoil design and general flow conditions this can lead to pressure side flow separation and increased suction side peak Mach numbers.

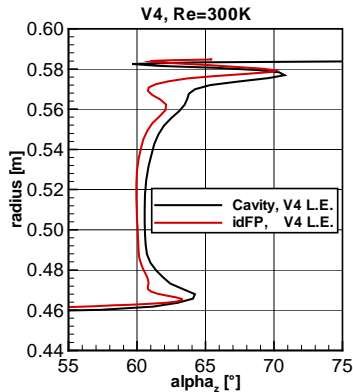


Figure 13: Comparison of radial distribution of yaw angle at vane 4

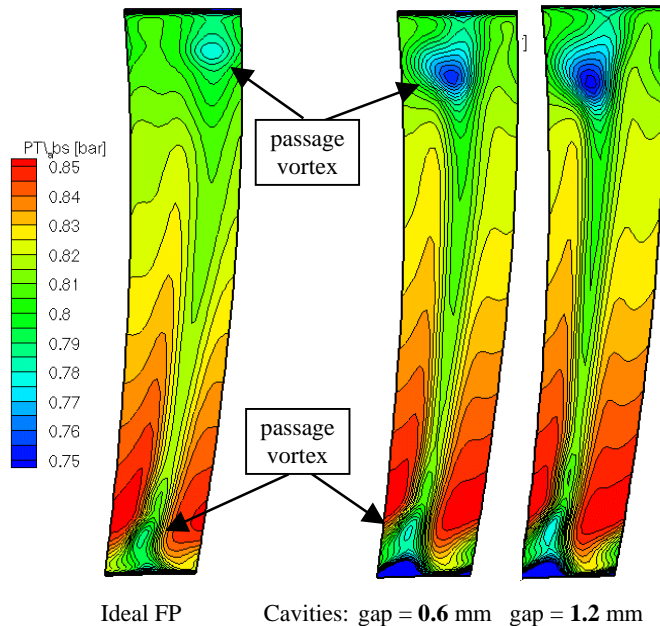


Figure 14: Total pressure distribution in axial plane downstream of vane 4 (V4)

Furthermore the fluid leaving the cavity has gathered a higher entropy. At the vane tip sections the upstream outer air seal releases a thickened boundary layer caused by the leakage and the related mixing losses. This thicker vane inlet boundary layer intensifies the formation of the passage vortex system in the tip region of the vanes (except of

course for the first vane). This effect can already be obtained from figure 6 but becomes more obvious from figure 14.

It is important to note that at the tip the passage vortex related pressure minimum is not only more pronounced but that it moved quite a way radially into the main flow. This means that the passage vortex in this vane not only collects less energetic fluid but really gains strength. This can be expected to cause additional losses inside the vane and the subsequent rows. At the hub this effect is much smaller. Here, a part of the inlet boundary layer is sucked into the hub cavity upstream of the vane significantly reducing the effect of a disturbed vane inlet boundary layer.

In the case of the reduced clearance gaps (0.6 mm) the secondary flow pattern looks very much like the reference gap case (1.2 mm). The intensity of the passage vortex is somewhat reduced and also the distance the vortex core has moved into the flow channel. However, qualitatively it is not half way between the full gap and the ideal flow path. It is concluded thereupon, that there is a loss mechanism involved, which is not primarily dependent on the leakage flow rate governed by the clearance.

EVALUATION OF CAVITY RELATED LOSS MECHANISMS

Leakage flow through the inner and outer air seals introduces several loss mechanisms, which reduce turbine performance. As discussed in the introduction several authors addressed cavity flow related losses. While Traupel [11] reports more integral loss increase, Denton [12] puts a special focus on the mixing losses of the re-entering leakage flow without mentioning flow field changes and losses in subsequent rows. Wallis et al. [13] mention four losses, which are losses at cavity entry, sealing fins, mixing losses of re-entering flow and incidence related losses in subsequent rows.

Based on the observations of this study combined with the findings in literature five groups of cavity related losses are identified. First effect is the “by-pass” effect of the leakage flow. The leakage flow does not reduce its enthalpy level like the main flow although it is subject to approximately the same pressure drop. In terms of the enthalpy-entropy diagram the flow through the labyrinth seals equals a horizontal line from row inlet to exit pressure, resulting in an entropy rise depending on the pressure difference.

For stator vanes this results in a reduction in exit velocity for a fixed mass flow. In rotor blades the work extraction is reduced. This results in a reduced isentropic efficiency, because due to the pressure drop across the clearances the overall pressure ratio and thus the isentropic power is not equally reduced as the real power output. Hence, this “by-pass” effect can be viewed either as reduced work output by reduced enthalpy reduction or as increased losses through a flow fraction, which changes pressure only by loss generation across clearance fins. Since losses occurring in the entry region of a cavity contribute to the overall cavity throughflow, they can be combined with the clearance losses.

Another loss mechanism, which is considered to be very significant in literature is the mixing losses connected to the velocity differences between the re-entering cavity flow and the main flow. For these Denton [12] provides a simple estimate for the momentum losses due to mixing.

A third loss generation process is surely the windage by differently rotating walls inside the cavities. A fourth loss source appear to be the

steps in the flow path, which will be discussed further below. Finally the presence of cavity leakage flows changes the inflow to the subsequent airfoil rows as seen in the last section. These “subsequent row losses” are mainly incidence and secondary flow losses, which including their interdependence not only depend on the cavity exit flow but also on the airfoil and turbine design parameters.

Relative magnitude of cavity related loss mechanisms

In this chapter the attempt is being made to get an estimate of the relative magnitude of the five above mentioned loss mechanisms for the investigated turbine. These considerations are based on the numerical simulation combined with analysis. Although such a simulation definitely does not capture all complex physical effects, based on the verification step, it is claimed that it captures the main flow characteristics necessary for this analysis to be reasonably valid. The division between ideal conditions and real conditions will be made by comparing the ideal flow path and the cavity computations for the intermediate Reynolds number case.

The losses attributed to cavity induced effects are related to the losses generated by the main flow in the ideal flow path computation, which can be computed by the following approach:

According to Denton [12] the enthalpy loss coefficient ζ is quantitatively equivalent to the entropy loss coefficient ζ_s .

$$\zeta_s \approx \zeta = \frac{h_2 - h_{2is}}{h_{12} - h_2} \quad (3)$$

$$\text{with : } h_{12} - h_2 = \frac{1}{2} v_2^2$$

For the ideal flow path computation and this point of operation the average loss coefficient for the airfoils was

$$\bar{\zeta} \approx 0.05$$

With this a total enthalpy loss for the 3-stage turbine can be computed:

$$\Delta h_{loss, row} = \bar{\zeta} \cdot \frac{v_2^2}{2} = 1 \frac{kJ}{kg} \quad (\text{with : } v_2 \approx 200 \frac{m}{s}) \quad (4)$$

$$\Delta h_{loss, LPT} = 6 \cdot \Delta h_{loss, row} = 6 \frac{kJ}{kg}$$

This number is quite close to the equivalent number based on the individual airfoil losses. In order to quantify the loss associated with the “by-pass” effect it is assumed that the pressure drop is hardly changed by the by-pass, which means that a horizontal line can be drawn in the h-s diagram for the leakage flow. This means that the overall enthalpy drop in the airfoil row is reduced by this amount of leakage flow. Hence a simple formula can be set up:

$$\Delta h_{loss, row, by-pass} = \frac{\dot{m}_L}{\dot{m}_m} \cdot \Delta h_{row} \quad (5)$$

In the test turbine reaction was close to 50 % except for the first stage. Using the simulation data the “by-pass” loss can be estimated as:

row	Δh_{row} [kJ/kg]	m_L/m_m row	Δh_{loss} row [kJ/kg]
B3	8	0.0070	0.056
V4	10.5	0.0047	0.049
B4	10.5	0.0073	0.077
V5	11	0.0038	0.042
B5	11	0.0074	0.081
LPT		-	0.305

Table 2: Enthalpy loss of “by-pass” mechanism (5)

Relating this result to the total loss generated by the airfoils in the ideal flow path this loss amounts to 5 % of the main flow loss for the current configuration.

To estimate the mixing losses of the re-entering flow the momentum loss formula of Denton [12] is used. It is given by:

$$\zeta_{mix} = \frac{T\Delta s}{0.5 \cdot v_2^2} = \frac{v_2^2}{2} \cdot \frac{\dot{m}_L}{\dot{m}_m} \left[v_{\theta 2}^2 \left(1 - \frac{v_{\theta L}}{v_{\theta 2}} \right) + v_{x2}^2 \left(1 - \frac{v_{xL}}{v_{x2}} \right) \right] \quad (6)$$

In figures 15 and 16 the axial and absolute circumferential velocities are shown for OAS1 and IAS2. Plugging in these velocities according to equation (6) the following loss coefficients are evaluated:

row	seal	ζ_{mix} row
B3	OAS1	0.008
V4	IAS2	0.007

Table 3: Loss coefficient based on equation (6)

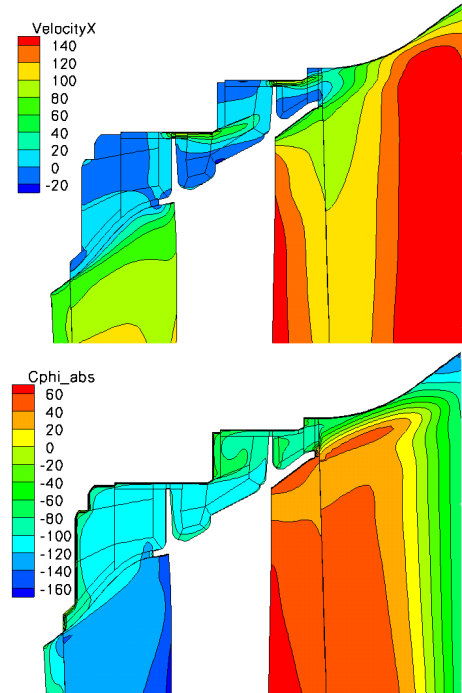


Figure 15: Axial and absolute circumferential velocity in OAS1 (Blade 3) in [m/s]

Interestingly both loss coefficients are very similar, although the relative leakage fraction of the outer air seal is about 50 % higher. The reason is that for the same leakage flow the mixing is more intensive at the hub due to the larger velocity differences between cavity exit and main flow.

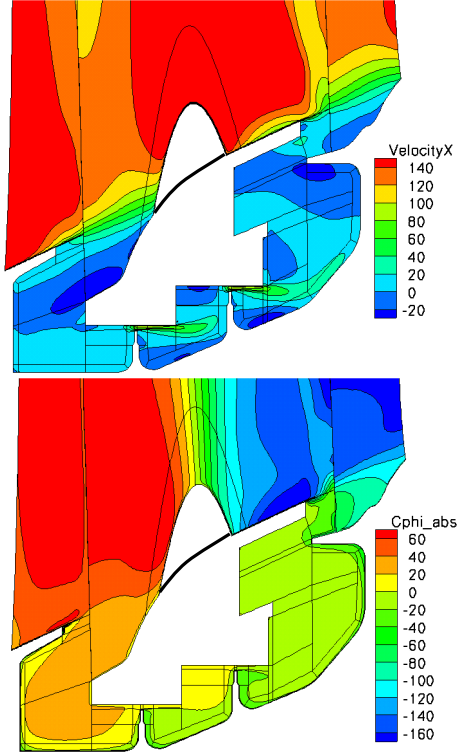


Figure 16: Axial and absolute circumferential velocity in IAS2 (Vane 4) in [m/s]

Using the ζ -values evaluated in the first blade and second vane cavity combined with the same average exit velocity as in equation (4) for all vanes and rotors, respectively, the overall mixing loss of the re-entering flow can be estimated to:

$$\Delta h_{loss,mix} = \sum_{rows} \zeta_{loss,mix,row} \cdot \frac{1}{2} \bar{v}_2^2 = 0.76 \frac{kJ}{kg} \quad (7)$$

This number corresponds to approximately 12.5 % of the losses in the ideal flow path.

The windage losses can be estimated through the total temperature change between inlet and exit of the cavities. In the outer air seals this temperature drops by approximately 0.3 K, while the temperature rises in the inner air seal by approximately 3 K. The difference between inner and outer air seals is actually not surprising. In the outer air seals the absolute circumferential velocity is slightly larger than the rotation velocity of the outer shroud (appr. 100 m/s), actually leading to a small amount of work extraction. At the hub, however, the rotation and the absolute velocity of the flow leaving the rotor in the main stream is of opposite sign. Thus the velocity difference is about 120 m/s. Using the temperature differences the loss generation due to windage in the hub cavities can be estimated:

$$\Delta h_{windage,vane} = \frac{m_L}{m_m} \cdot c_p \Delta T_t = 0.004 \cdot 1.0045 \cdot 3 \approx 0.012 \frac{kJ}{kg} \quad (8)$$

For two inner air seals (Vane 4 & 5) this is equivalent to 0.4 % of the loss in the ideal flow path. Hence, although the windage losses quantification is quite heavily depending on the accuracy of the numerical solution, which cannot be expected to be very precise for the loss-related flow details inside the cavities, the windage losses can be expected to be approximately one order of magnitude smaller than “by-pass” losses and mixing losses.

Originally the working hypothesis in this investigation was that there are only four loss mechanisms and the fourth mechanism is the “subsequent row losses”, which could be approximated by subtracting the first three loss types from the whole difference between ideal flow path and cavity computation. However, when the result of the simulation with the reduced gap came out at some point in the investigation, this result mismatched the original expectation.

Actually the total loss increase between ideal flow path and cavity computation turned out to be $\Delta h = 1.6$ kJ/kg. Reducing the gap by half only recovered approximately $\Delta h = 0.45$ kJ/kg instead of 0.8 kJ/kg, which would be exactly in the middle (figure 17). In terms of efficiency this means that even if the clearances were zero there would still be a significant efficiency difference between ideal and cavity geometry (dashed line extension).

The “by-pass” and the mixing loss according to equations (5) and (6) depend linearly on the leakage flow fraction. Since the leakage flow is reduced by 50 % in the reduced gap case, these loss components in first order are also reduced by half, i.e. from together $\Delta h = 1.06$ kJ/kg to $\Delta h = 0.53$ kJ/kg (red triangle in figure 17). This is slightly more than the $\Delta h = 0.45$ kJ/kg computed by the numerical simulation. At least partially this could be explained by the further reduction of the axial velocity component of the re-entering leakage flow and its influence on the mixing loss. Reducing the clearance gaps to zero should reduce these two loss components to zero, thus leaving about $\Delta h = 0.6$ kJ/kg unexplained, since no obvious mechanism could be identified, which explains an equivalent increase of secondary flow losses (According to figure 14 the passage vortex seems even to be reduced for the 0.6 mm gap case.).

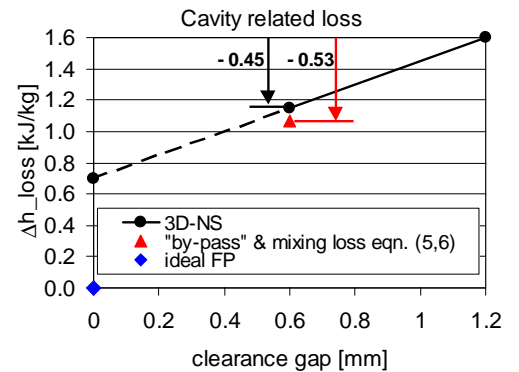


Figure 17: Cavity related losses for turbine

The only cause for this additional loss appear to be the steps in the real flow path. For example downstream of the first rotor (B3) the flow duct features a backward facing step at the hub, in which the entry

vortex of the inner air seal is located. Such steps are present at all cavity inlets and exits. In a first order approximation these steps can be viewed as causing a Carnot loss depending on the area ratio:

$$\zeta_c = \frac{\Delta p}{\rho/2 v_1^2} = \left(1 - \frac{A_1}{A_2}\right)^2 \quad (9)$$

Actually equation (9) describes a pressure loss and not an enthalpy or entropy loss, but the difference for these flows is surely much smaller than the approximation quality of simple one-dimensional estimates. Furthermore this loss cannot be used for the re-entering cavity flows, since these are captured in equation (6) characterising the mixing losses.

Hence, only the 5 cavity entries and the first vane inner air seal exit (no leakage) can be taken for this loss estimate in the cases with flow through the seals. With an approximate average area ratio of 1.07 for each step, based on the geometrical difference between upstream and downstream area of the steps, it can be estimated:

$$\Delta h_{loss,steps} = \zeta_c \cdot v_x^2 \approx 0.07 \cdot \left(100 \frac{m}{s}\right)^2 \approx 0.05 \frac{kJ}{kg} \quad (10)$$

$$\Delta h_{loss,steps,total} = \sum_{steps} \Delta h_{loss,steps} = 6 \cdot 0.05 \frac{kJ}{kg} = 0.3 \frac{kJ}{kg}$$

With this result the loss breakdown in table 4 is obtained. For the "subsequent row losses", for which no direct evaluation seems feasible, the losses of the first four effects are subtracted from the overall loss change between ideal flow path and cavity computation:

	Δh [kJ/kg]	$\Delta h / \Delta h_{total}$ [%]
total Δ (idealFP - Cavity)	1.6	100.0
"by-pass" losses	0.3	18.8
mixing losses @ re-entry	0.76	47.5
windage	0.04	2.5
"step losses"	0.3	18.8
"subsequent row losses"	0.2	12.5

Table 4: Relative fraction of cavity related losses

This means that at nominal clearances the mixing losses make up about 50 % of the cavity related losses and thus the largest part. The "by-pass" losses and the "step losses" turn out to be of the same magnitude for the given clearance gap. The "subsequent row losses", which mainly include incidence and secondary flow losses are somewhat smaller.

	gap = 1.2 mm	gap = 0.6 mm	gap = 0 mm
	Δh [kJ/kg]	Δh [kJ/kg]	Δh [kJ/kg]
total Δ (idealFP - Cavity)**	1.6	1.15	0.7
"by-pass" losses	0.3	0.15	0
mixing losses @ re-entry	0.76	0.38	0
windage	0.04	0.04	0.04
"step losses"	0.3	0.35	0.5
"subsequent row losses"	0.2	0.23	0.16

**.: result of numerical simulation, gap = 0 extrapolated

Table 5: Stack-up of cavity related losses for different clearance gap configurations

For the extreme (theoretical) case of vanishing clearance gaps the "by-pass" losses and the mixing losses have to approach zero. On the other hand the "step losses" will increase, since now also the cavity exits form flow path steps without throughflow.

For the vanishing gaps the "step losses" increase is estimated to $\Delta h = 0.2$ kJ/kg, because only 5 additional steps have to be taken into account and the step height is somewhat smaller for the re-entry steps.

It would be alternatively possible to split the mixing losses into the circumferential mixing losses and the axial mixing losses and to integrate the "step losses" into the axial mixing.

The resulting stack-up for the three gap cases is reported in table 5. The "step-loss" value for the reduced gap is slightly modified, modelling that the mixing in the re-entry is already increased by the reduced seal throughflow. The "subsequent row losses" remain fairly constant, but this is of course depending on the estimate of the other loss components.

The essence of this loss evaluation is that the pure presence of the real cavities and their platforms introduces losses, referred to as "step losses", which also induce additional secondary flow losses. Their presence is also responsible for the fact, that the passage vortex in the second vane does not change that much between the two gap cases. They also cause the large difference between the two cavity computations on one side and the ideal flow path computation on the other side in terms of radial efficiency distribution (fig. 5). The magnitude of these losses will heavily depend on the platform design and steepness of the flow duct and thus will be different for different turbine designs. It should be also mentioned that losses due to circumferential in- and outflow in the cavity – main flow path connection occur, which are difficult to accurately assess in a steady-state computation. To assess this a fully coupled unsteady simulation would be needed. The influence of these circumferential non-uniformities will have to be included in one of the discussed loss mechanisms or assessed separately.

To conclude this loss evaluation it should be noted that it is based on a numerical simulation and is performed for a given test turbine. Changing the design parameters of the turbine will surely affect this loss breakdown to a certain extent, it being a change in the relative magnitudes between the different loss components or between total cavity losses and ideal flow path losses.

CONCLUSIONS

In this paper the interaction between the main flow and the leakage flow in a shrouded turbine has been investigated for an aero engine low pressure turbine rig. To assess the quality of the numerical simulation on which the analysis is based, the measured data gathered in the main flow was compared to the computation. In addition, plausibility checks were performed to judge the cavity computation details in absence of very fine experimental cavity data. Both checks revealed a pretty reasonable computation quality.

The investigation showed that there are significant interaction effects between main and cavity flow. As frequently described in literature, the leakage flow resulted in an incidence change for the subsequent airfoil row. Furthermore it became obvious that the increased thickness of the inlet boundary layer to the subsequent row caused an intensification of the passage vortex system in this

subsequent row. These mechanisms also cause a radial shift in the mass flow distribution.

An attempt was made to separate different loss mechanisms in this investigation. These mechanisms are referred to as “by-pass” loss, mixing loss of the re-entering flow, windage losses, “step losses” and “subsequent row losses”, the latter combining losses due to incidence and increased secondary flows.

The main result of this analysis was that the mixing losses amounted to about 50 % of the total cavity related losses, while the “by-pass” and “step losses” made up approximately 20 % of the cavity losses. Losses due to incidence and secondary flows were estimated to have a smaller fraction. The windage losses came out fairly negligible.

The “step losses” become stronger in cases with reduced leakage flow and are strongly dependent on the main turbine design features.

Further work in this area can focus on further improving simulation quality based on more detailed measurements and investigation of other typical turbines. Also it could be worthwhile looking into effects of unsteadiness.

ACKNOWLEDGEMENT

The numerical work, especially the upgrading of the computation methodology, was funded by the German Ministry of Commerce within the E3E UPDATE program. The authors wish to thank MTU Aero Engines for permission to publish this paper.

REFERENCES

- [1] Egli, A., 1935, “The Leakage of Steam through Labyrinth Seals”, *Trans. of the ASME*, Vol. 57, pp 115-122
- [2a] Rhode, D.L., Johnson, J.W., Broussard, D.H., 1996, “Flow Visualization and Leakage Measurements of Stepped Labyrinth Seals; Part 1: Annular Groove”, *ASME paper 96-GT-136*, IGTI congress, Birmingham, UK
- [2b] Rhode, D.L., Younger, J.S., Wernig, M.D., 1996, “Flow Visualization and Leakage Measurements of Stepped Labyrinth Seals; Part 2: Sloping Surfaces”, *ASME paper 96-GT-137*, IGTI congress, Birmingham, UK
- [3] Takenaga, H., Matsuda, T., Yokota, H., 1998, “An Experimental Study on Labyrinth Seals for Steam Turbines”, *Proceedings, 8th International Symposium on Flow Visualisation*, Sorrento, Italy
- [4] Millward, J.A., Edwards, M.F., 1994, “The Windage Heating of Air Passing through Labyrinth Seals”, *ASME paper 94-GT-56*
- [5] Denton, J.D., Johnson, C.G., 1976, “An Experimental Study of the Tip Leakage Flow around Shrouded Turbine Blades”, CEGB research report CEGB-R/M/N848
- [6] Pfau A., Treiber M., Sell M., Gyarmathy G. 2000, “Flow Interaction from the Exit Cavity of an Axial Turbine Blade Row Labyrinth Seal”, *ASME paper 2000-GT-481*
- [7] Peters, P., Breisig, V., Giboni, A., Lerner, Ch., Pfof, H., 2000, “The Influence of the Clearance of Shrouded Rotor Blades on the Development of the Flowfield and Losses in the Subsequent Stator”, *ASME paper 2000-GT-478*
- [8] Anker, J.E., Mayer, J.F., 2002, “Simulation of the Interaction of Labyrinth Seal Leakage Flow and Main Flow in an Axial Turbine”, *ASME paper GT-2002-30348*
- [9] Korschunov, B.A., Döhler, S.W., 1996, “Einfluß von Leckageströmungen an der Laufradspitze auf die aerodynamischen Charakteristiken des folgenden Leitgitters”, *BWK Bd. 48*, pp. 49-55
- [10a] Hunter, S.D., Manwaring, S.R., 2000, “Endwall Cavity Flow Effects on Gaspath Aerodynamics in an Axial Flow Turbine: Part 1 – Experimental and Numerical Investigation”, *ASME paper 2000-GT-651*
- [10b] Hunter, S.D., Manwaring, S.R., 2000, “Endwall Cavity Flow Effects on Gaspath Aerodynamics in an Axial Flow Turbine: Part 2 – Source Term Model Development”, *ASME paper 2000-GT-513*
- [11] Traupel, W., 1966, “Thermische Strömungsmaschinen”, Springer Verlag
- [12] Denton, J.D., 1993, “Loss Mechanisms in Turbomachines”, *ASME paper 93-GT-435*
- [13] Wallis, A.M., Denton, J.D., Demargne, A.A.J., 2000, “The Control of Shroud Leakage Flows to Reduce Aerodynamic Losses in a Low Aspect Ratio, Shrouded Axial Flow Turbine”, *ASME paper 2000-GT-475*
- [14a] McLean, Ch., Camci, C., Glezer, B., 2001, “Mainstream Aerodynamic Effects Due to Wheel-space Coolant Injection in a High-Pressure Turbine Stage: Part 1: Aerodynamic Measurements in the Stationary Frame”, *J. of Turbomachinery*, Vol. 123, pp 687-696
- [14b] McLean, Ch., Camci, C., Glezer, B., 2001, “Mainstream Aerodynamic Effects Due to Wheel-space Coolant Injection in a High-Pressure Turbine Stage: Part 2: Aerodynamic Measurements in the Rotational Frame”, *J. of Turbomachinery*, Vol. 123, pp 697-703
- [15] Girgis, S., Vlastic, E., Lavole, J-P., Moustapha, S.H., 2002. “The Effect of Secondary Air Injection on the Performance of a Transonic Turbine Stage”, *ASME paper GT-2002-30340*
- [16] Wellborn, S.R., Okiishi, T.H., 1999, “The Influence of Shrouded Stator Cavity Flows on Multistage Compressor Performance,” *J. of Turbomachinery*, Vol. 122
- [17] Demargne, A.A.J., Longley, J.P., 2000, “The Aerodynamic Interaction of Stator Shroud Leakage and Mainstream Flows in Compressors,” *ASME Paper 2000-GT-570*
- [18] Wellborn, S.R., 2001, “Details of Axial-Compressor Shrouded Stator Cavity Flows”, *ASME Paper 2001-GT-495*
- [19] Fritsch, G., Hoeger, M., Blaha, C., Bauer, D., 1997, “Viscous 3D Compressor Simulations on Parallel Architectures”, *AIAA Paper 97-2876*
- [20] Wilcox, D.C., 1988, “Reassessment of the Scale Determining Equation for Advanced Turbulence Models”, *AIAA Journal*, Vol. 25, No. 11, pp. 1299 – 1310
- [21] Gier, J., Ardey, S., Heisler, A., 2000, “ Analysis of Complex Three-Dimensional Flow in a Three-Stage LP Turbine by means of Transitional Navier-Stokes Simulation”, *ASME Paper 2000-GT-645*
- [22] Abu-Ghannam, B.J., Shaw, R., 1980, “Natural Transition of Boundary Layers – The Effects of Turbulence, Pressure Gradient and Flow History, *J. of Mechanical Engineering Science*, Vol. 22, No. 5, pp. 213 – 228
- [23] Drela, M., 1995, “Implementation of Modified Abu-Ghannam/Shaw Transition Criterion”, MIT Aero-Astro
- [24] Gier, J., Ardey, S., 2001, “On the Impact of Blade Count Reduction on Aerodynamic Performance and Loss Generation in a Three-Stage LP Turbine”, *ASME Paper 2001-GT-197*